Supporting Information

A Hydrazone Schiff Base as a Fe(III) Sensor and Precursor to a Violet-Emissive Mn (II) Complex: Synthesis, Crystal Structure, Luminescence, Supramolecular and DFT Studies

Muhammad Lauqman,[a] Nida Javaid,[b] Mubashar Ilyas,[a] Muhammad Nawaz Tahir,[C] Muhammad Ashfaq,[C] Junaid Ali,[d] Madiha Saqlain,[a] and Hui Li,*[a]

[a] Key Laboratory of Clusters Science of Ministry of Education, School of Chemistry and Chemical Engineering, Beijing Institute of Technology, Beijing, 100081, P. R. China.

[b] Department of Botany, Government College University Faisalabad, Faisalabad 38000, Pakistan

[c] Department of Physics, University of Sargodha, Sargodha 40100, Pakistan

[d] Department of Chemical Sciences, University of Naples Federico II, 80126 Naples, Italy

Corresponding author name and Email:

Hui Li (lihui@bit.edu.cn)

Table of Contents

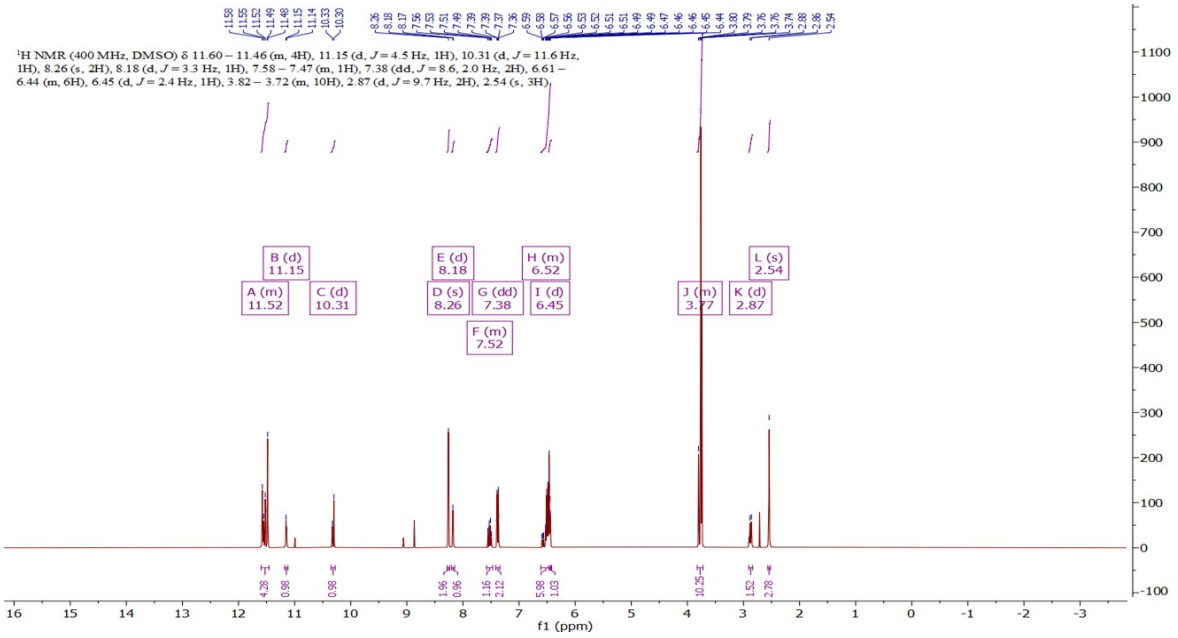

Figure S1. [1]H NMR of Ligand HL

¹H NMR (400 MHz, DMSO-d⁶, δ ppm): 11.52 (1H, Ar–OH, H_A), 11.15 (1H, N–H_hydrazone, H_B), 10.31 (1H, N–H_amide, H_C), 8.26 (1H, Ar–H, H_D), 8.18 (1H, Ar–H, H_E), 7.52 (1H, Ar–H, H_G), 7.38 (1H, Ar–H, H_F), 7.58–7.47 (1H, Ar–H), 6.61 (1H, Ar–H), 6.52 (1H, Ar–H, H_H), 6.45 (1H, Ar–H, H_I), 3.72–3.22 (10H, OCH_3 + CH_2, H_J), 2.87 (2H, CH_2–CO, H_K), 2.54 (3H, OCH_3, H_L).

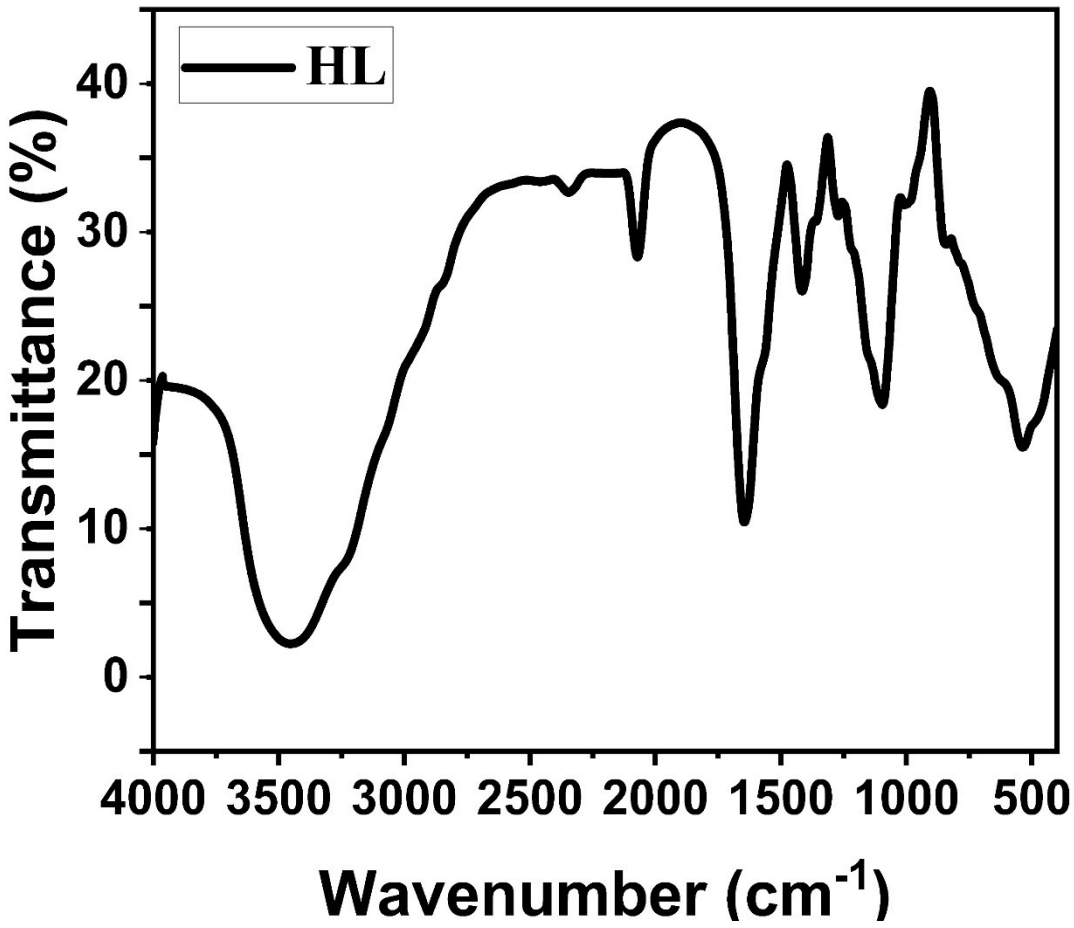

Figure S2. FT-IR Spectrum of HL Ligand

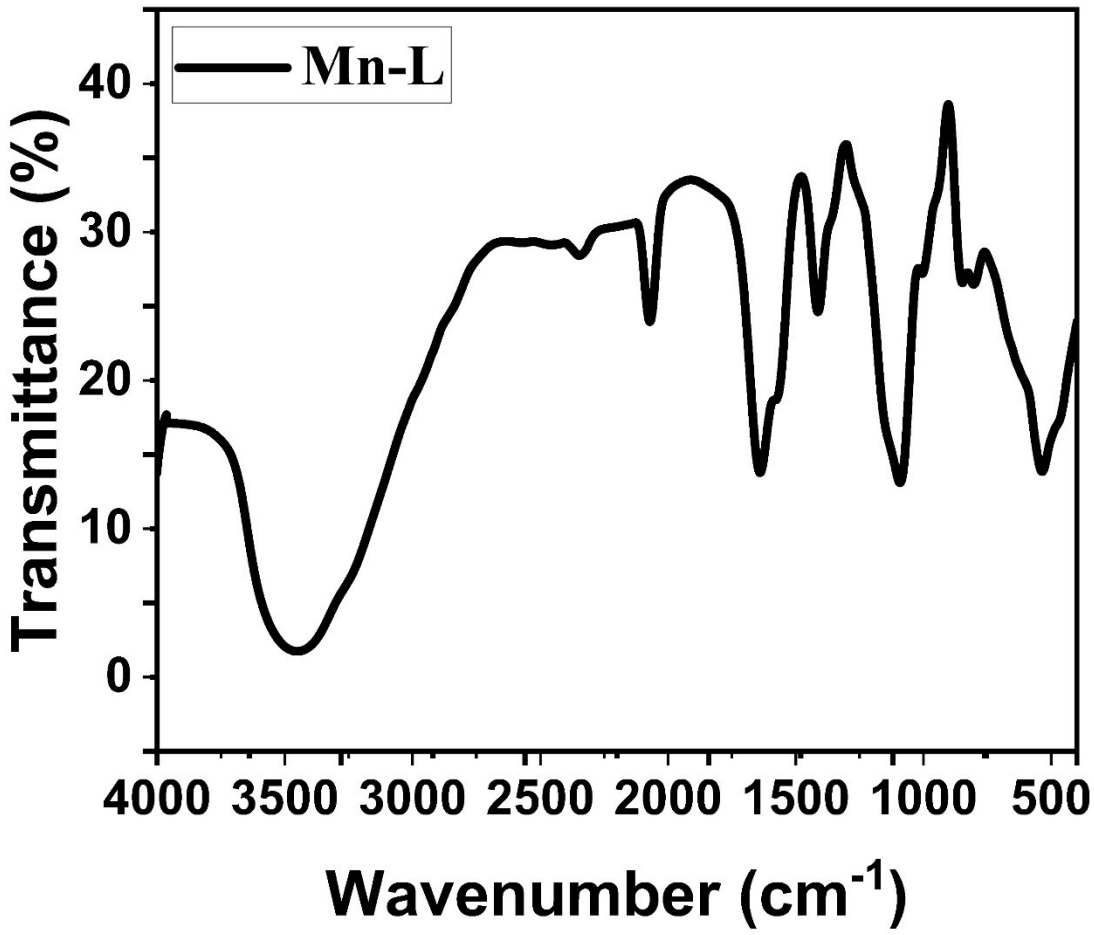

Figure S3. FTIR Spectrum of Complex Mn-L

Characteristic bands for ν(O–H/νN–H) at around 3400 cm^{-1}, ν(C=O) at about 1650–1700 cm^{-1}, and ν(C=N) stretching of the azomethine group at about 1610 cm^{-1} are visible in the HL ligand's FTIR spectrum. These bands move to lower frequencies when complexed with Mn, indicating that the azomethine nitrogen and carbonyl oxygen coordinate with the Mn core. Furthermore, the Mn–L complex exhibits novel absorptions in the 600–500 cm^{-1} range, which are ascribed to stretching vibrations between Mn–N and Mn–O. These spectrum shifts verify that the Mn–L combination was successfully coordinated and formed.

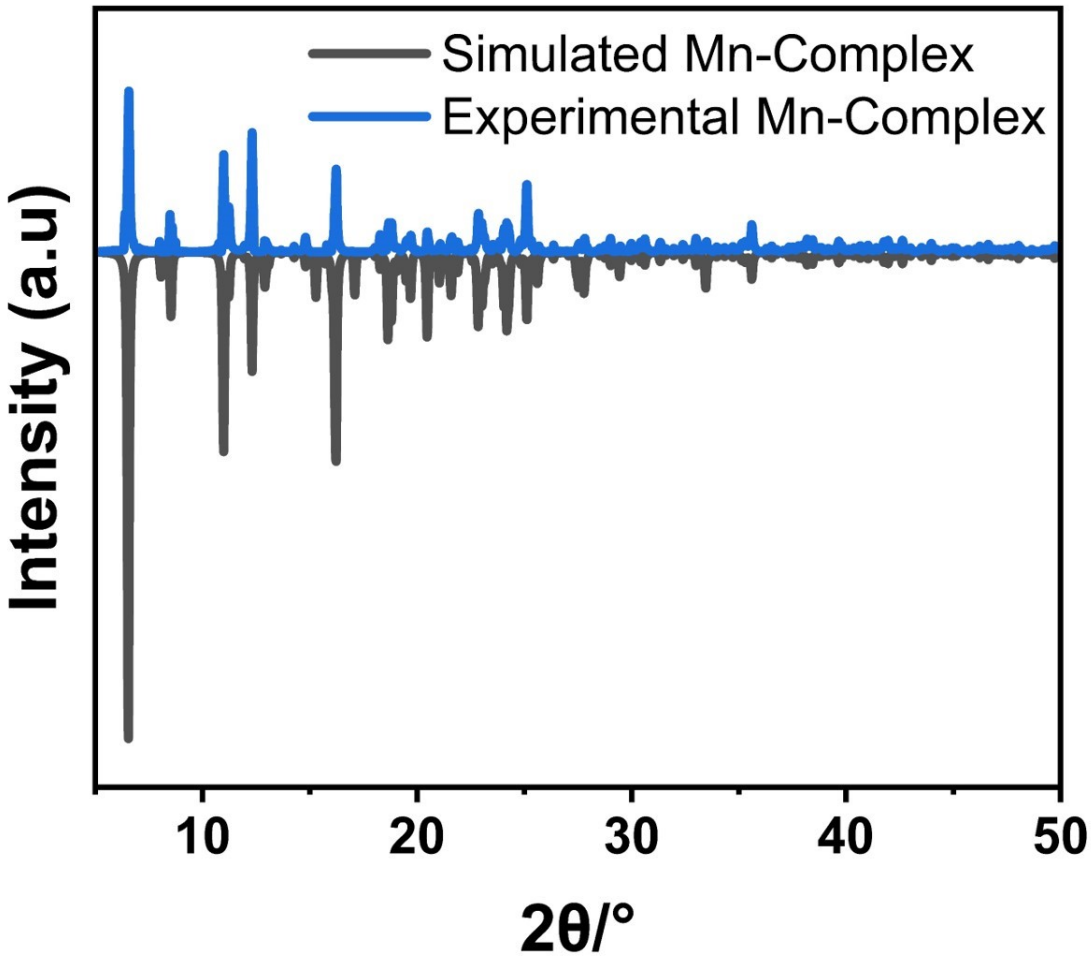

Figure S4. The experimental and simulated PXRD Pattern of Complex Mn-L

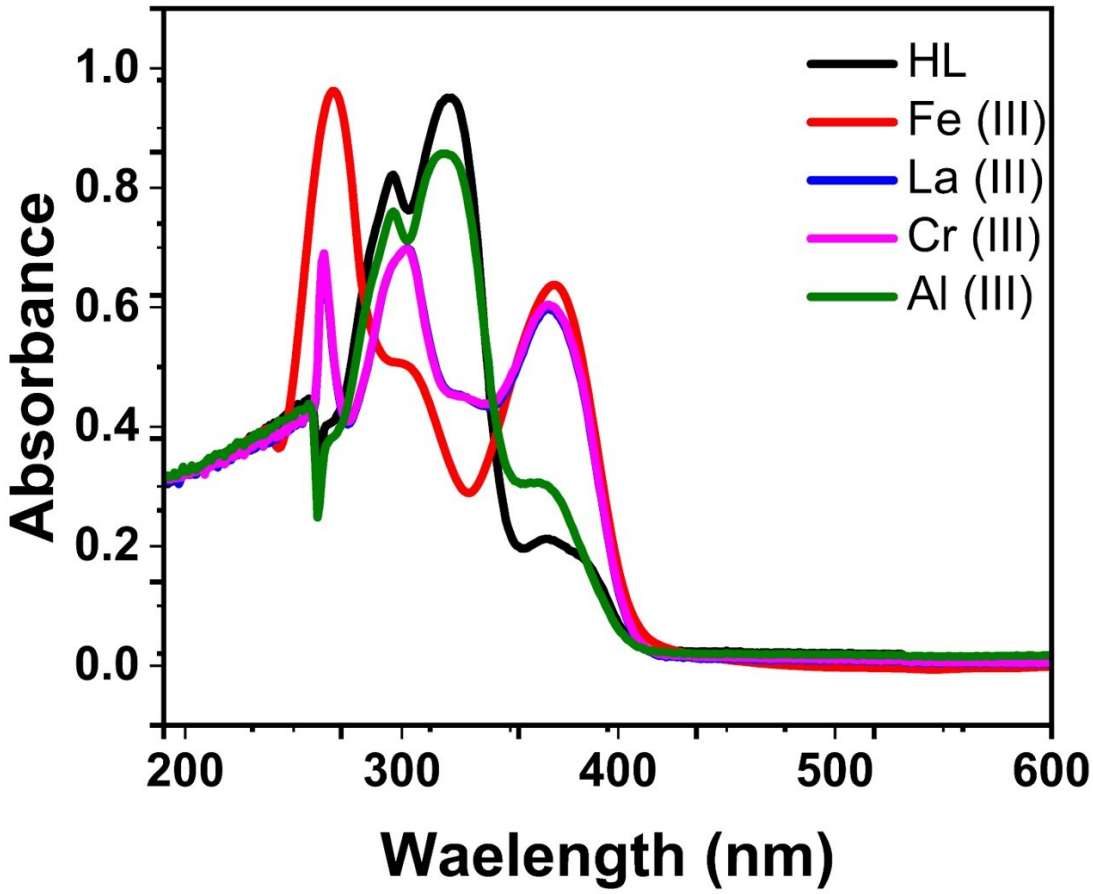

Figure S5. The interaction of HL with Trivalent metal ion

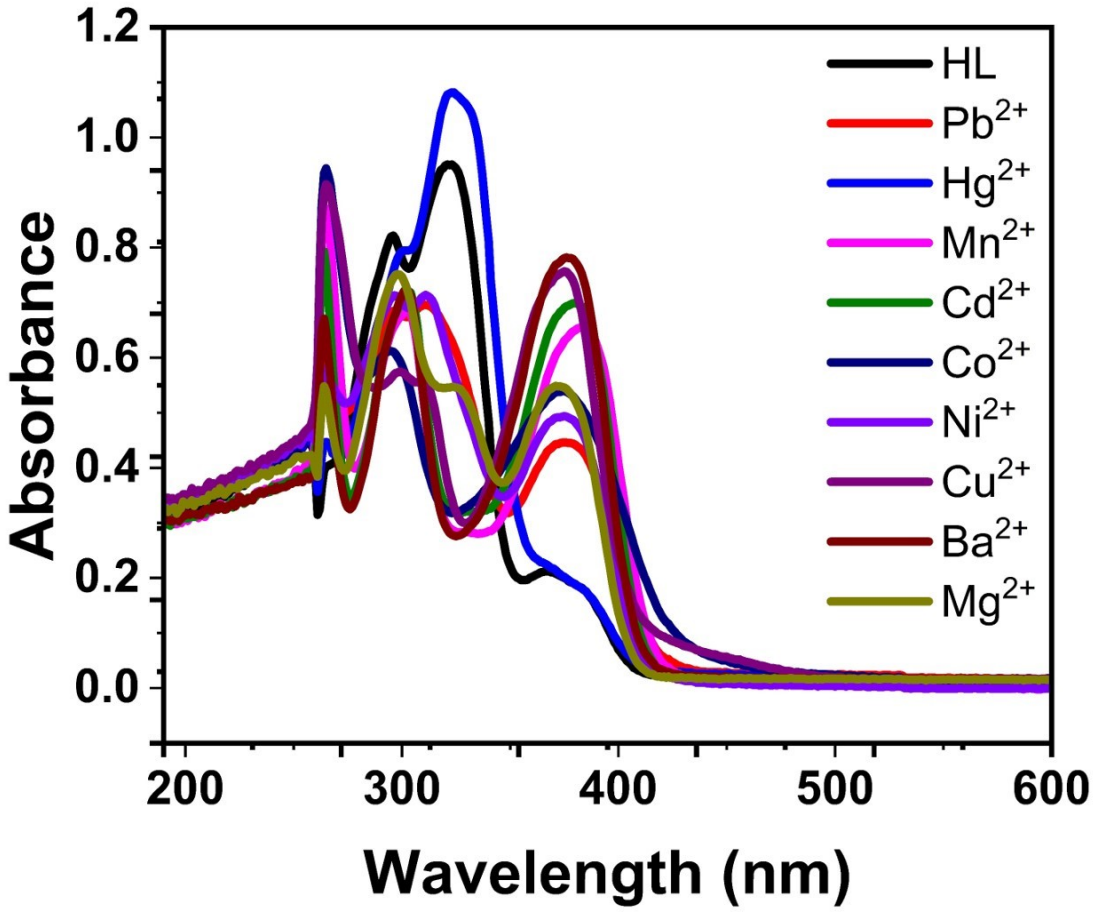

Figure S6. The interaction of HL with divalent metal ions

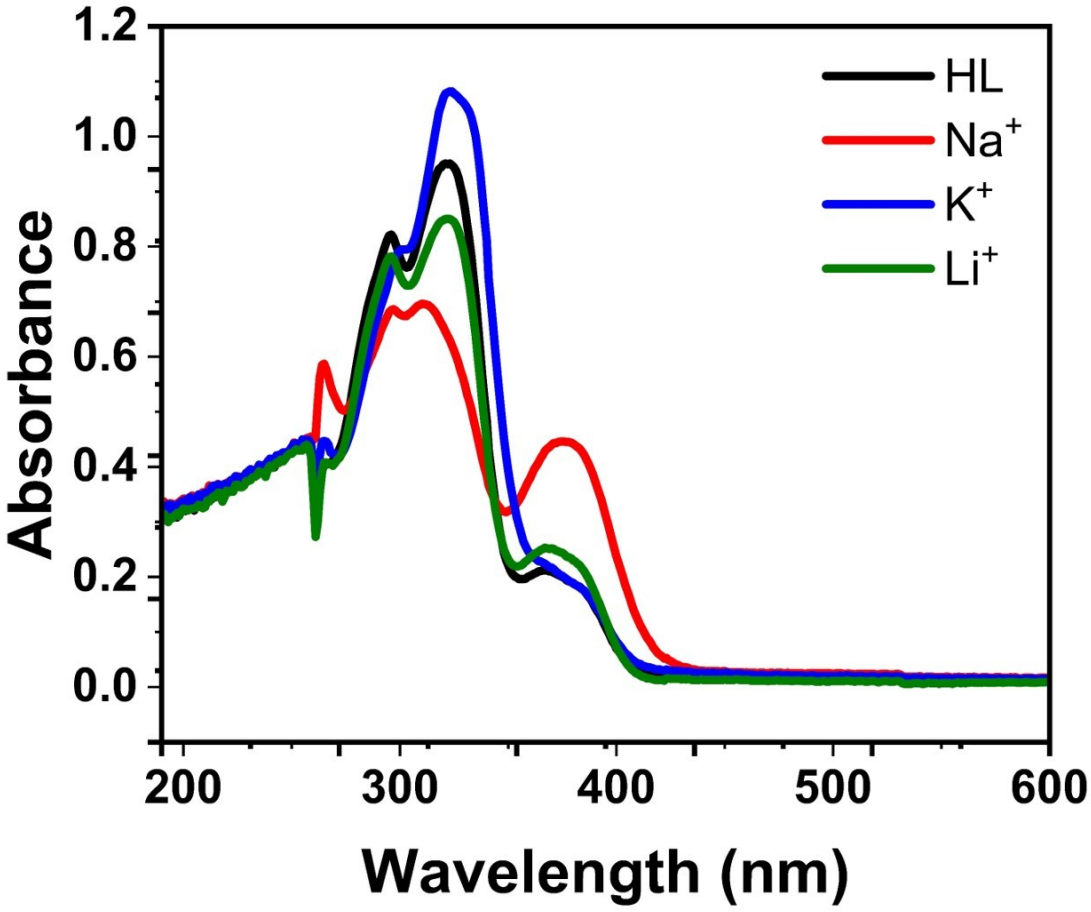

Figure S7. The interaction of HL with monovalent metal ions

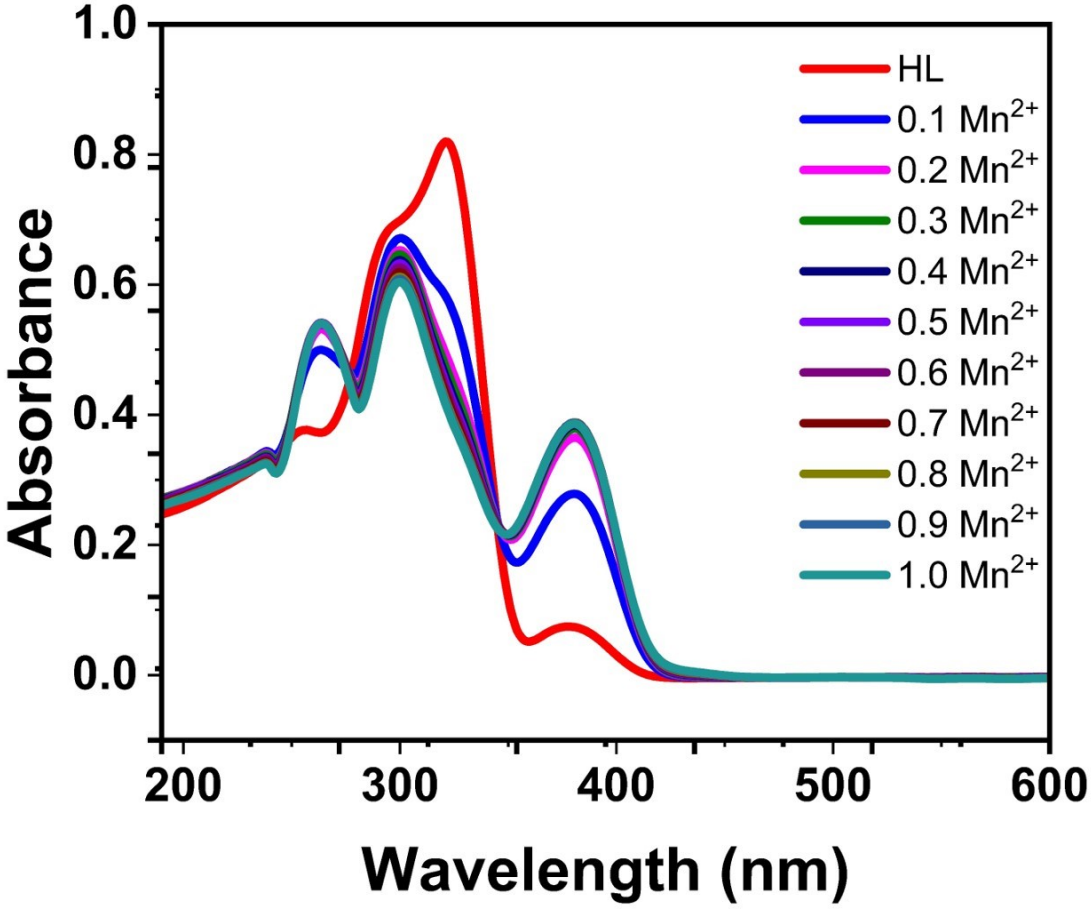

Figure S8. The HL Ligand Titration with Manganese metal

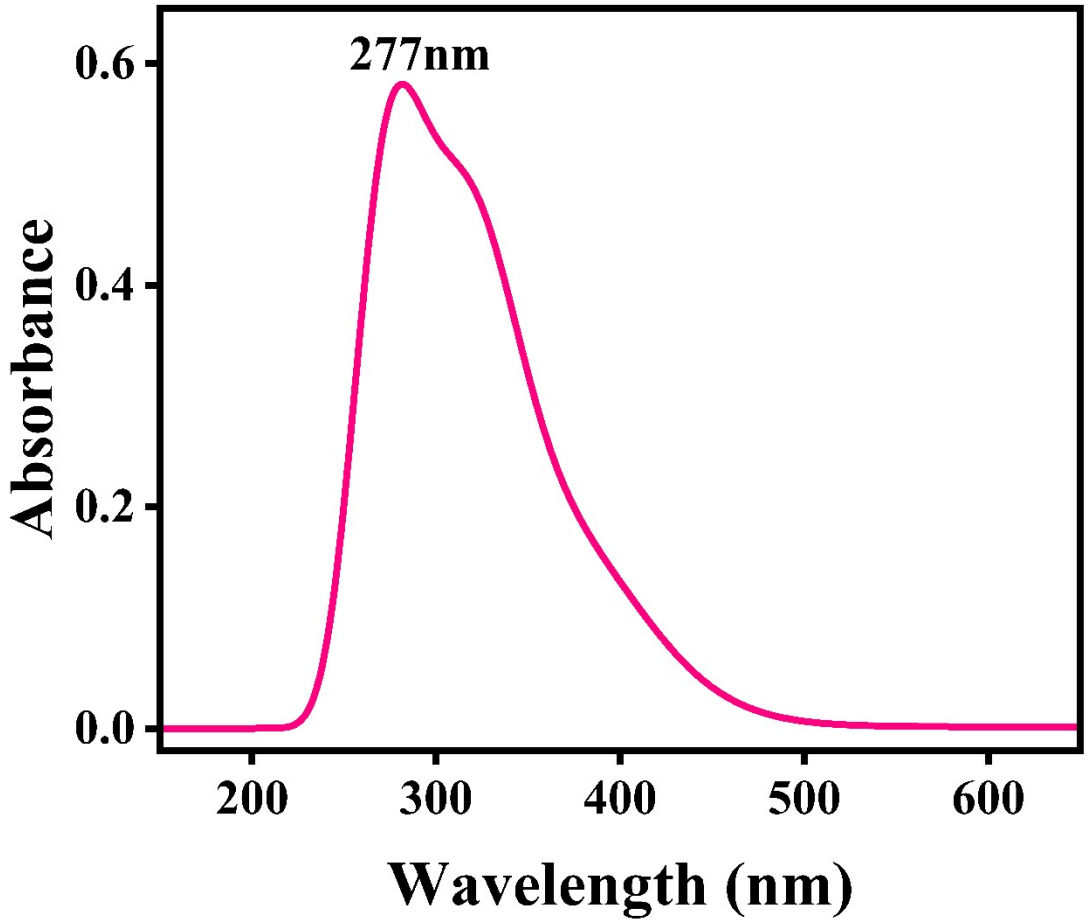

Figure S9. Simulated UV-Visible Spectrum for Complex Mn-L in DMF

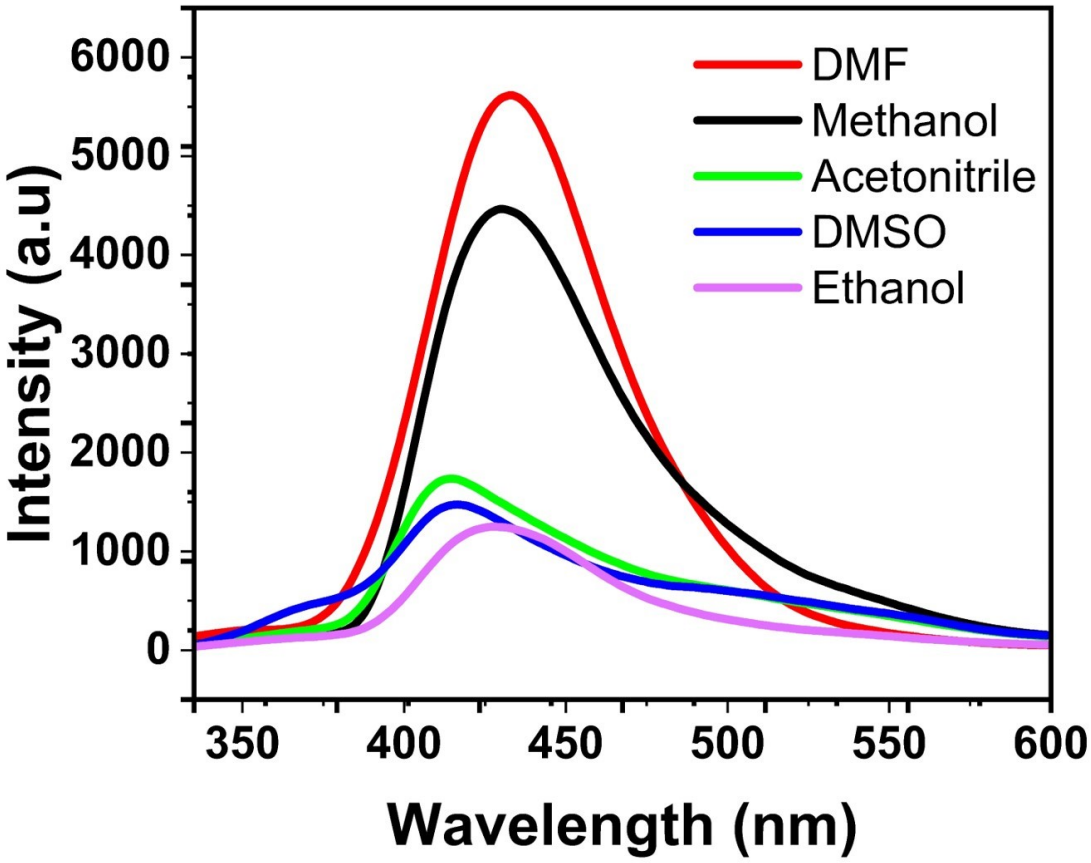

Figure S10. The PL Spectra of HL Ligand in different Solvents s

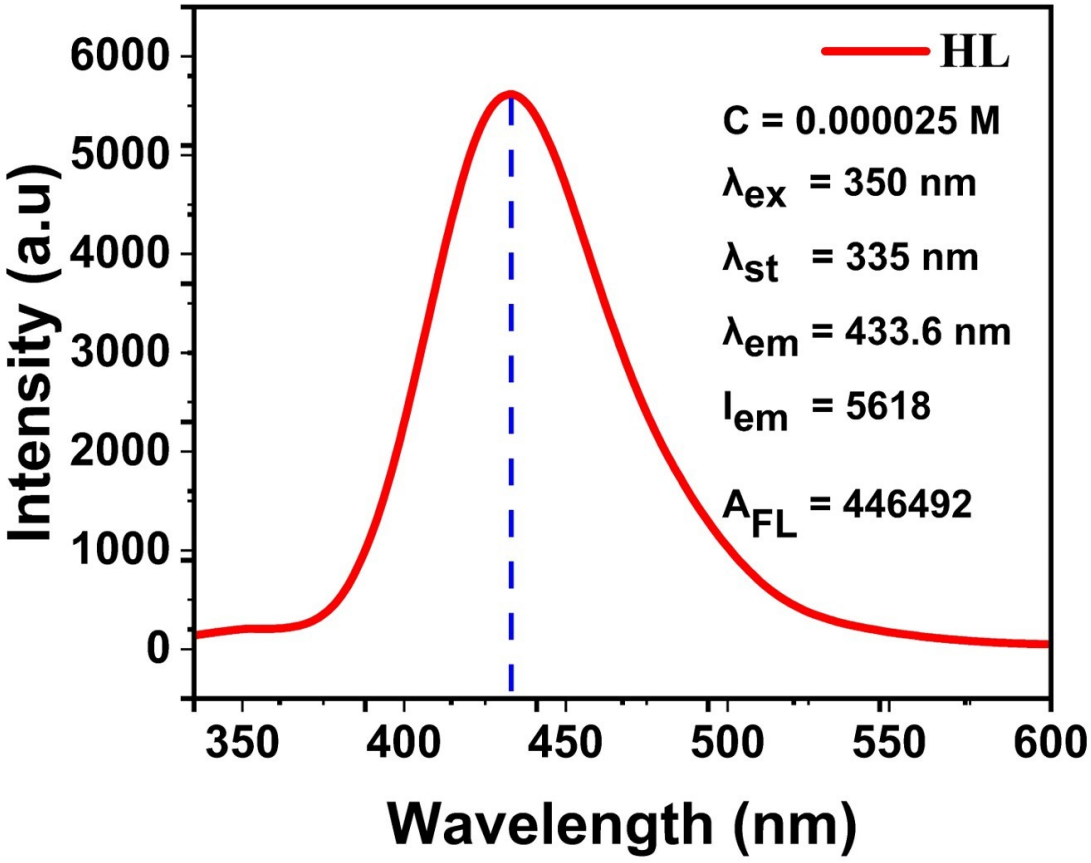

Figure S11. The HL Ligand Area under PL Curve

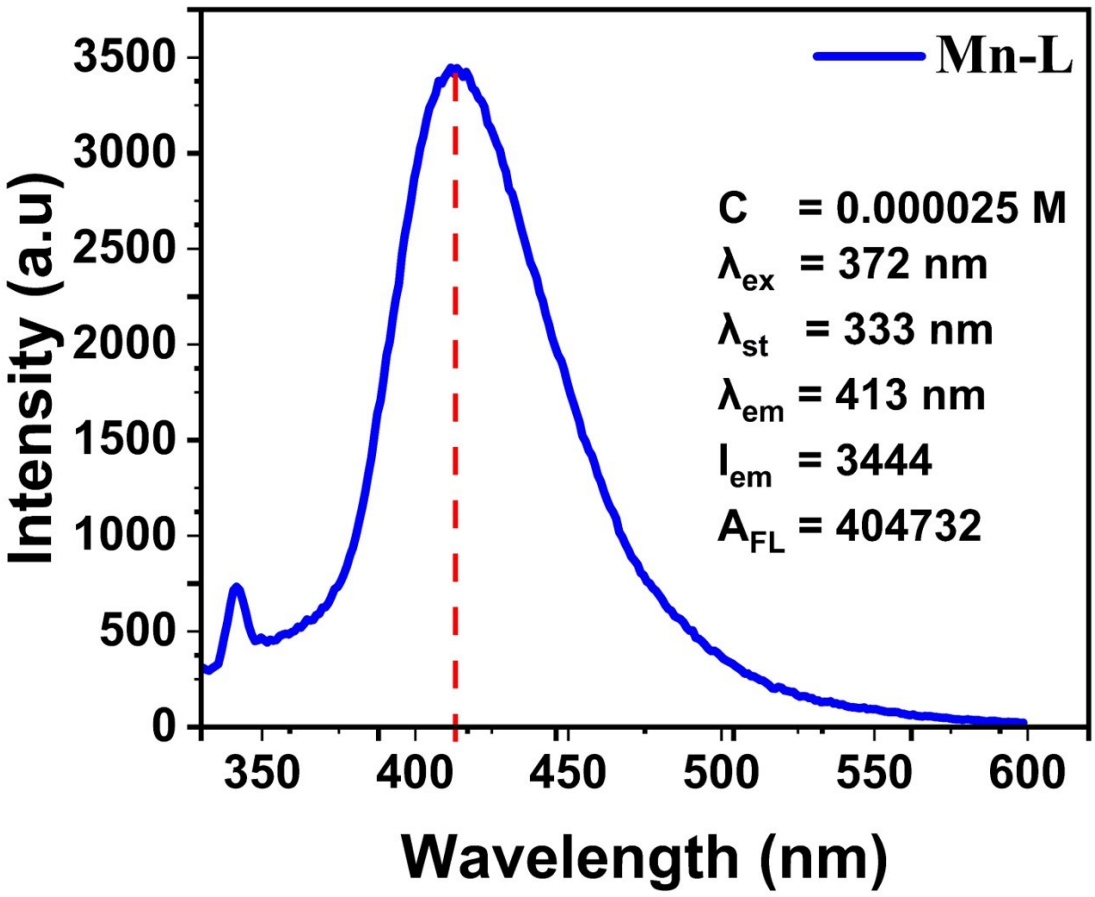

Figure S12. Complex Mn-L Area under PL Curve

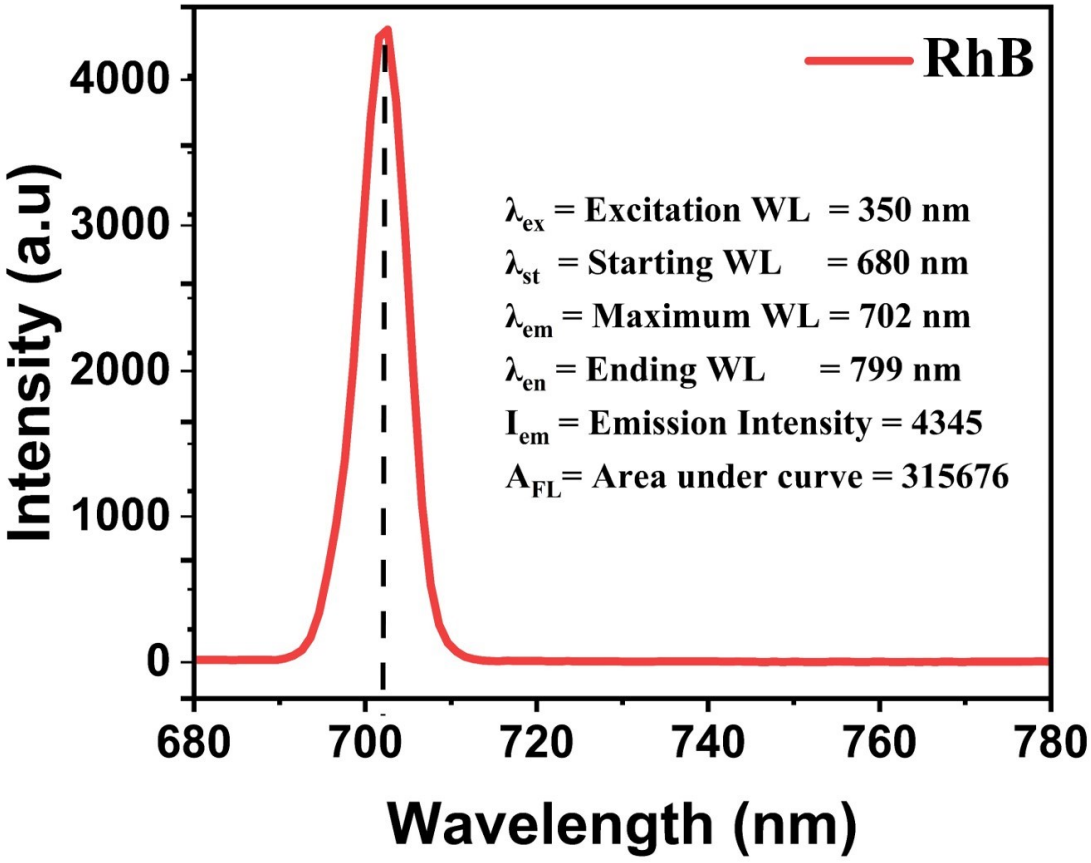

Figure S13. Rhodamine B Area under PL Curve

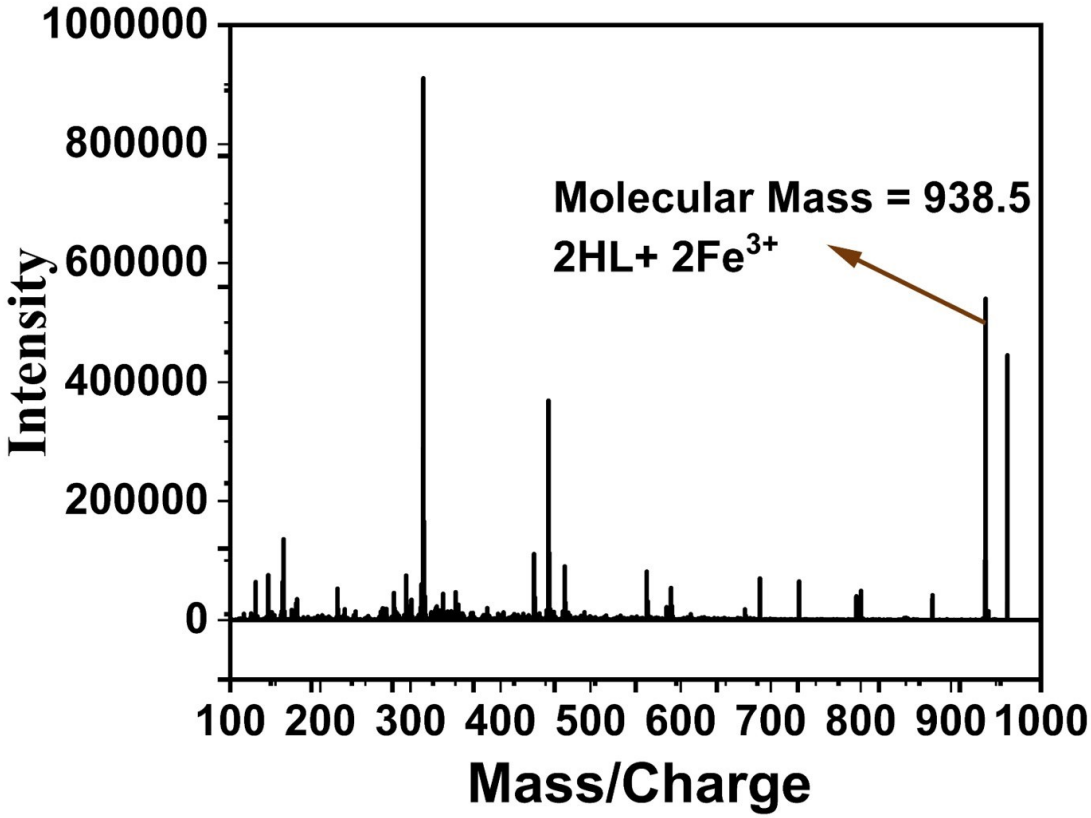

Figure S14. ESI-MS Spectrum of $2HL+2Fe^{3+}$ Complex

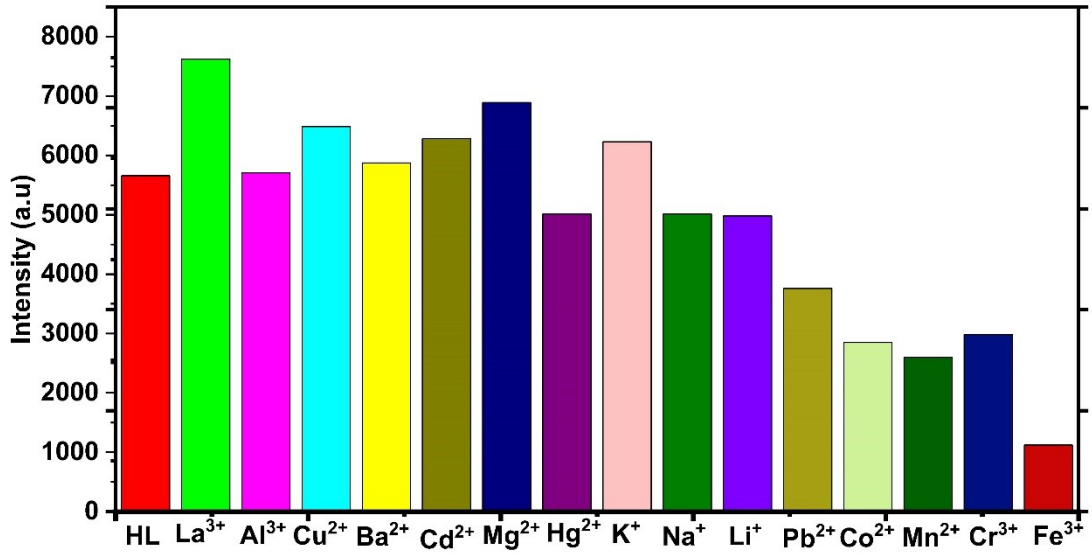

Figure S15. Anti-Interference experiment for Fe^{3+} detection

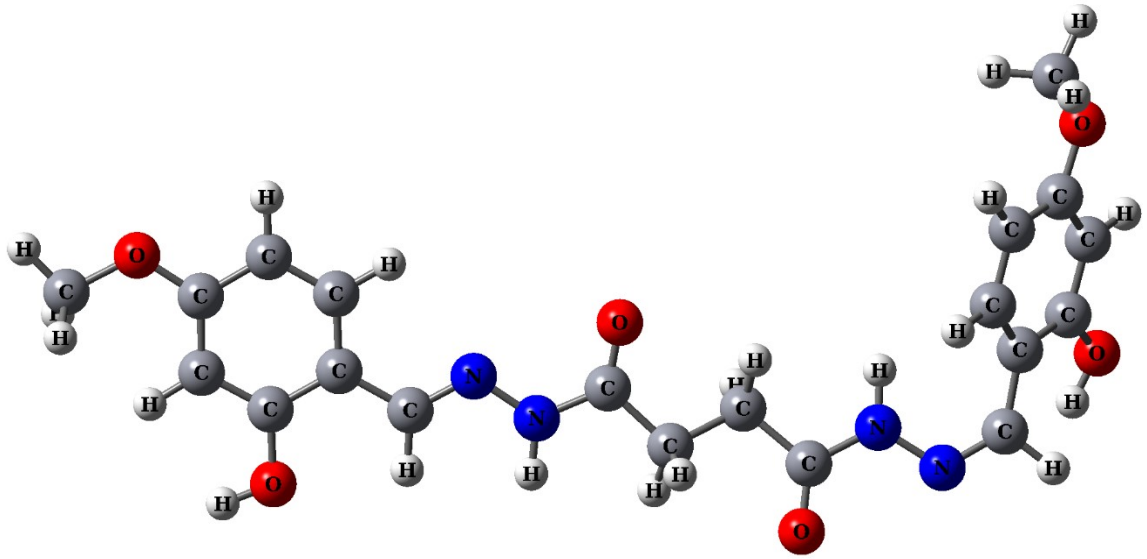

Figure S16. The optimized structure of Ligand HL

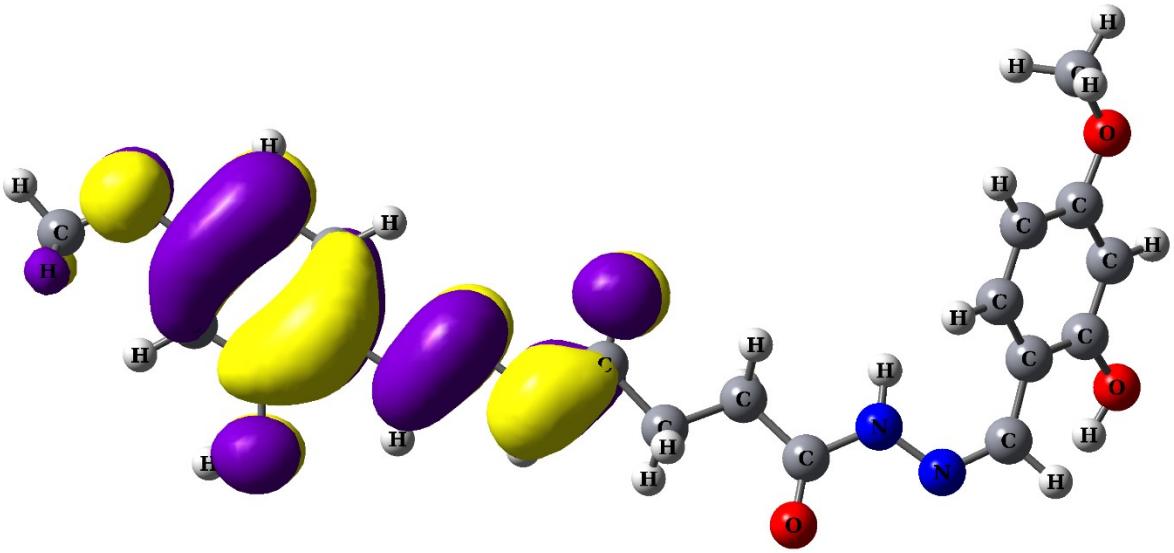

Figure S17. HOMO of Ligand HL

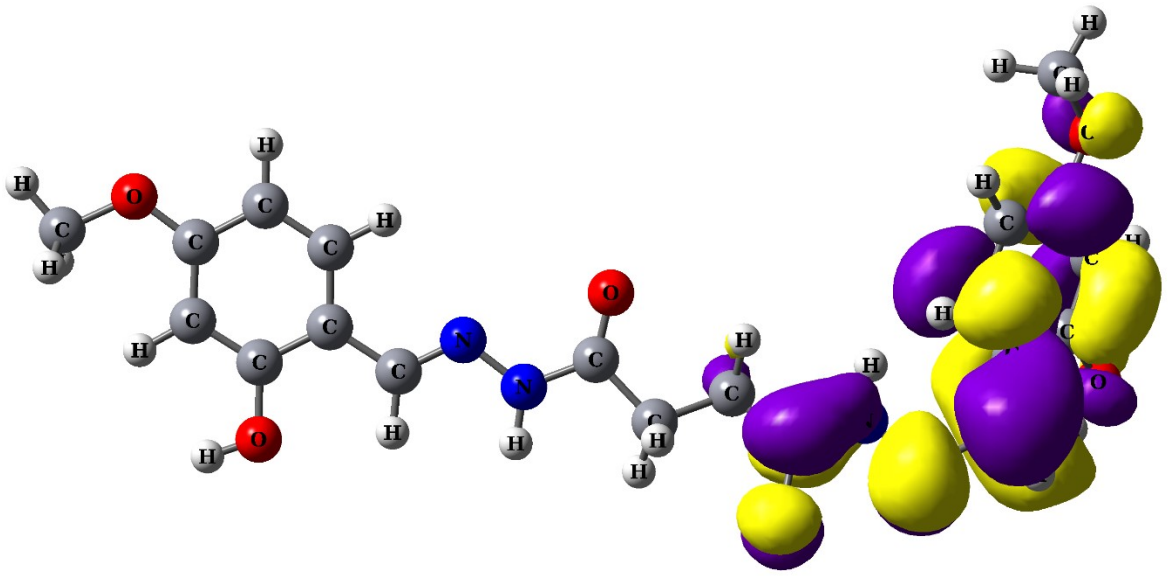

Figure S18. HOMO of Ligand HL

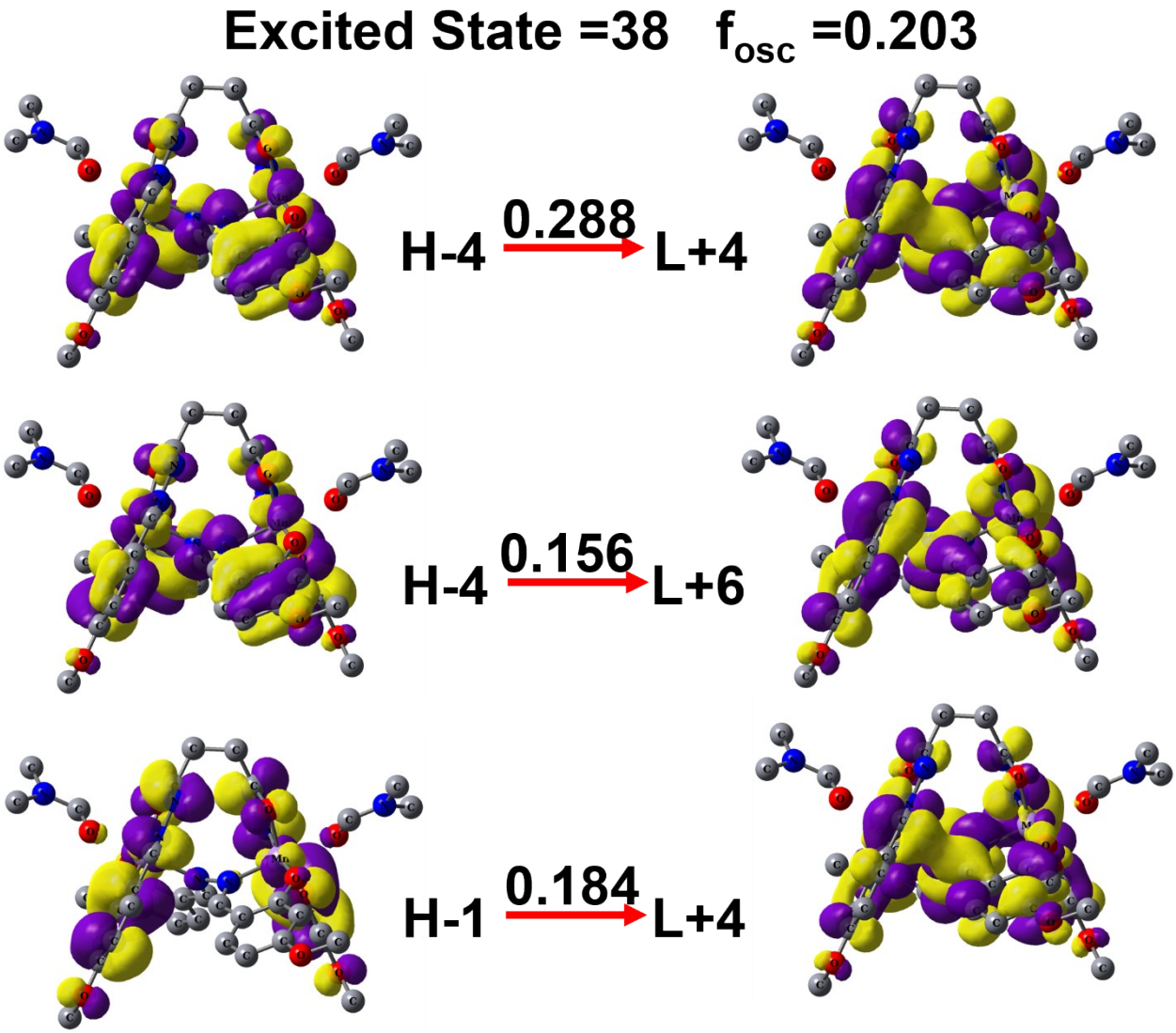

Figure S19. 38th excited state of Mn-L

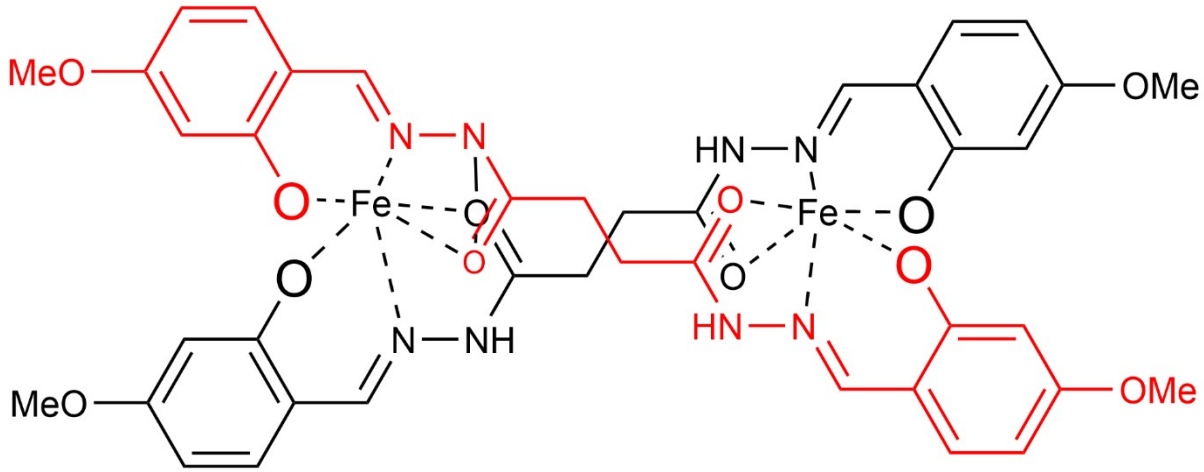

Figure S20. The Possible binding mode between HL and Fe(III)

Table S1. Vital important bond lengths (Å) and bond angles (°) of **Mn-L Complex**.

Bond	**Experimental**	**Theoretical**	**Bond Angle**	**Experimental**	**Theoretica**
Mn1—O2	1.898 (3)	1.865	O2—Mn1—O3	94.58 (16)	94.35
Mn1—O3	1.903 (3)	1.892	O2—Mn1—O4	95.14 (18)	96.25
Mn1—O4	1.922 (4)	1.896	O3—Mn1—O4	170.26 (18)	169.21
Mn1—N3	1.962 (5)	2.026	O2—Mn1—N3	173.30 (18)	172.12
Mn1—O1	2.286 (4)	2.147	O3—Mn1—N3	90.06 (18)	89.21
Mn1—N2	2.314 (4)	2.006	O4—Mn1—N3	80.3 (2)	79.54
O1—C1	1.241 (6)	1.237	O2—Mn1—O1	87.04 (15)	86.75
O2—C4	1.307 (6)	1.315	O3—Mn1—O1	92.82 (15)	91.56
O3—C12	1.320 (6)	1.300	O4—Mn1—O1	88.39 (15)	87.12
O4—C20	1.311 (8)	1.306	N3—Mn1—O1	87.90 (16)	86.78
O5—C14	1.358 (9)	1.419	O2—Mn1—N2	85.27 (14)	84.90
O5—C19	1.421 (11)	1.418	O3—Mn1—N2	92.42 (14)	92.10
O6—C6	1.361 (6)	1.398	O4—Mn1—N2	87.68 (14)	87.25
O6—C11	1.438 (7)	1.419	N3—Mn1—N2	99.38 (15)	98.97
N1—C1	1.312 (7)	1.348	O1—Mn1—N2	171.02 (14)	170.59
N1—C2	1.440 (9)	1.456	C1—O1—Mn1	123.1 (4)	122.51
N1—C3	1.448 (8)	1.452	C4—O2—Mn1	136.3 (3)	135.4
N2—C10	1.282 (6)	1.313	C12—O3—Mn1	129.6 (3)	128.9
N3—C18	1.277 (7)	1.297	C20—O4—Mn1	112.5 (4)	111.7
N3—N4	1.426 (7)	1.393	C14—O5—C19	118.2 (7)	117.6
N4—C20	1.285 (9)	1.304	C6—O6—C11	117.0 (5)	116.5

Table S2. Enrichment ratio for atomic pairs with random contact greater than 0.98.

Contact %	**Atom**	**H**	**C**	**N**	**O**	**Mn**
	H	51.9	18.4	5.1	23.9	
	C	18.4	0.1	0.5		
	N	5.1	0.5	0.1		
	O	23.9				
	Mn					
Surface%		75.6	9.55	2.9	11.95	0
Random contacts %	**Atom**	**H**	**C**	**N**	**O**	**Mn**
	H	57.15				
	C	14.44	0.91			
	N	4.38	0.55	0.08		
	O	18.07	2.28	0.69	1.43	
	Mn	0.00	0.00	0.00	0.00	0.00
Enrichment ratio	**Atom**	**H**	**C**	**N**	**O**	**Mn**
	H	0.91				
	C	1.27				
	N	1.16				
	O	1.32	0.00		0.00	
	Mn					

Table S3. Comparison of the present work with other fluorescent receptors for the selective detection of Fe(III)

Structure of Probe	Method	LOD	Binding Constant	Solvent	Ref
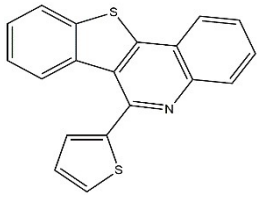	Flourescence	6.3 µM	1.98×10^{4} M^{-1}	CH_3CN/H_2O	[1]
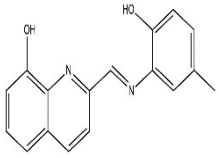	Flourescence	47 nM	2.06×10^{-8}	$DMSO/H_2O$	[2]
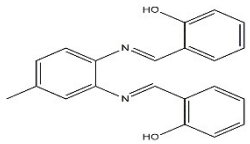	Flourescence	21.5 nM	2.7×10^{4} M^{-1}	CH_3CN/H_2O	[3]
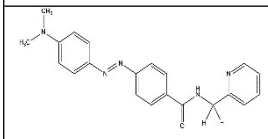	Flourescence	18 nM	1.0×10^{6}	CH_3CN/H_2O	[4]
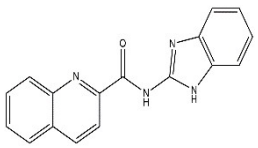	Flourescence	124 nM	5.1×10^{4} M^{-1}	H_2O	[5]
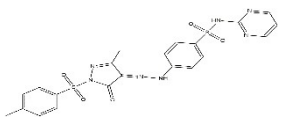	Flourescence	17 µM	Not Mentioned	CH_3OH	[6]
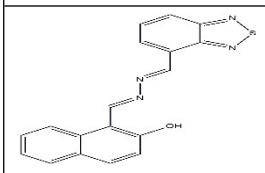	Flourescence	36 nM	8.41×10^{6}	H_2O	[7]
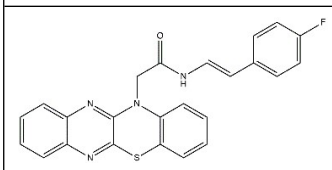	Flourescence	3.39 µM	1.13×10^{6} M^{-1}	CH_3OH	[8]
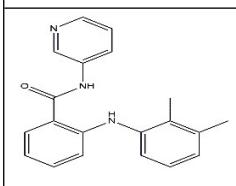	Flourescence Quenching	6 nM	2.14×10^{2} M^{-1}	DMF/H_2O	[9]

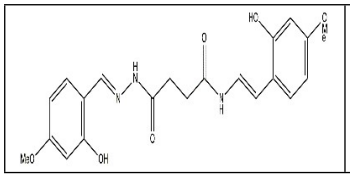	Flourescence Quenching	0.76 µM	2.74×10^5 M^{-1}	DMF	This Work

References

1. Patil, P., et al., *Benzothieno [c] quinoline based a novel fluorescent "turn-on" chemosensor for the detection of Fe (III) from aqueous solution.* Inorganica Chimica Acta, 2024. **573**: p. 122342.
2. Marimuthu, P., et al., *Design and synthesis of simple quinoline-based organic molecules as dual/multifunctional chemosensors for the detection of Cu2+/Fe3+ ions.* Journal of Molecular Structure, 2024. **1312**: p. 138530.
3. Lee, J.-S., et al., *A highly selective fluorescent probe for nanomolar detection of ferric ions in the living cells and aqueous media.* Arabian Journal of Chemistry, 2020. **13**(12): p. 8697-8707.
4. Saremi, M., A. Kakanejadifard, and M. Adeli, *A ratiometric fluorescent sensor based azo compound of 4-(4-Dimethylamino-phenylazo)-N-pyridin-2-ylmethyl-benzamide for rapid and selective detection of Fe3+ ion.* Journal of Molecular Liquids, 2022. **358**: p. 119168.
5. Zhang, B., et al., *A dual-response quinoline-based fluorescent sensor for the detection of Copper (II) and Iron (III) ions in aqueous medium.* Sensors and Actuators B: Chemical, 2017. **243**: p. 765-774.
6. Sayed, A., et al., *A novel fluorescent sensor for fast and highly selective turn-off detection of Fe3+ in water and pharmaceutical samples using synthesized azopyrazole-benzenesulfonamide derivative.* Journal of Molecular Structure, 2021. **1225**: p. 129175.
7. Musikavanhu, B., et al., *A naphthol hydrazone Schiff base bearing benzothiadiazole unit for fluorescent detection of Fe3+ in PC3 cells.* Spectrochimica Acta Part A: Molecular and Biomolecular Spectroscopy, 2023. **289**: p. 122242.
8. Narayan, L., et al., *Quinoxaline-linked N-acyl hydrazine: A "turn-off" fluorescent probe for the selective recognition of Fe3+ in real water samples.* Journal of Photochemistry and Photobiology A: Chemistry, 2024. **457**: p. 115857.
9. Saeed, S., et al., *J-aggregation based AIEE active smart organic fluorophore as Fe3+*

ions sensor: Ultrasensitive sensing of ferric ions with large stokes shift via chelation induced quenched fluorescence emission. Microchemical Journal, 2025: p. 115943.